Journal of Organometallic Chemistry 1048 (2026) 124048

Contents lists available at ScienceDirect

Journal of Organometallic Chemistry

journal homepage: www.elsevier.com/locate/jorganchem

New phosphorescent supramolecular *Re*-rectangles and their mixed-valent anions

Viktoria Ebel, Marcel Geppert, Niklas Bauch, Michael Linseis, Rainer F. Winter *

Fachbereich Chemie, Universität Konstanz, Universitätsstraße 10, D-78457, Konstanz, Germany

ARTICLE INFO

Keywords:
Rhenium
Metallamacrocycle
Electrochemistry
Spectroelectrochemistry
Phosphorescence
Mixed-valent

ABSTRACT

We report on the synthesis and characterization of two new macrocyclic, rectangular tetrarhenium complexes resulting from the {*Re*(CO)$_3$}$_2$(2,2′-bis(benzimidazolate)) precursor {*Re*(CO)$_3$}$_2$(BiBzIm) and the core-rigidified 4,4′-bipyridine-type bridging ligands thieno[2,3-c:5,4-c']dipyridine (complex **2a**) or 9-(4-methylthiophenyl)-9H-pyrrolo[2,3-c:5,4-c']dipyridine (complex **2b**). Both complexes undergo four consecutive one-electron reductions which are all centered on the diimine ligands. Redox splittings of the first pair of reductions are traced to electronic coupling in the mixed-valent state where the charges at the two diimine ligands, 0 and −1, (formally) differ. IR and UV/vis/NIR spectroscopic investigations on the neutral, the one-, and the two-electron reduced forms of these complexes characterize the singly reduced monoanions as moderately strongly coupled mixed-valent systems of Class II. Interestingly, the charge distribution parameter $\Delta\rho$ derived from IR spectroscopy of ca. 0.25 is roughly twice as large as the optically derived values of Hush's delocalization parameter α. Complexes **2a,b** are strongly phosphorescent at 77 K, with quantum yields of 62% for **2a** and 91% for **2b** Phosphorescence is retained at r. t., albeit with significantly reduced quantum yields of 1.1% and 2.0%, respectively.

1. Introduction

The purposeful synthesis of metallamacrocycles through coordination-driven self-assembly provides a straightforward access to a rich variety of structural motifs, each with its own inherent characteristic properties [1–5]. Over time the field has matured from the simple preparation and characterization to the targeted synthesis of metallamacrocyclic structures that are able to perform certain functions, such as ion sensing [6–7] or the selective binding of guest molecules [8–10]. Others have found applications in biomedical contexts, e. g. as anticancer agents, [11–13] or as luminescent materials [14–16]. Tetrarhenium complexes with two pairs of monoanionic bis(bidentately) coordinating chelate and bridging diimine ligands, so-called "*Re*-rectangles" of the generic structure in Scheme 1, rank among the early examples of such metallamacrocycles. Interest in these structures was spurred by their intriguing luminescent properties, [17–29] as well as by their utilization as structural templates for studying intramolecular through-space electron transfer between the diimine ligands in the one-electron reduced, mixed-valent (MV) state [22,30–32]. The rectangular molecular architecture provides a rather rigid, collateral arrangement of the diimine ligands while predefining their stacking distance through the appropriate choice of the bis(bidentately) coordinating dianionic bridging ligands that form the short edges. Their luminescent properties range from diimine ligand-based fluorescence to phosphorescence from excited ^{3}MLCT, ^{3}IL or ^{3}LL'CT states (MLCT = metal-to-ligand charge transfer, IL = intraligand, LL'CT = laterally bridging-to-diimine ligand charge transfer). Efficient intersystem crossing (ISC) in *Re*-rectangles relies on the large spin-orbit coupling constant of the rhenium ion (the so-called heavy atom effect) [33] and on energetically low-lying *Re*/ligand-to-diimine charge transfer (ML-L'CT) or *Re*-to-diimine excitations as well as the lowering of the energy difference between the first excited singlet and triplet state, $\Delta E_{S1\text{-}T1}$ [21,27,29,34–35].

In the present work we employed the diimine ligands thieno[2,3-c:5,4-c']dipyridine and the new carbazole-derived 9-(4-methylthiophenyl)-9H-pyrrolo[2,3-c:5,4-c']dipyridine in concert with the often employed {*Re*(CO)$_3$}$_2$(2,2′-bis(benzimidazolate)) precursor {*Re*(CO)$_3$}$_2$(BiBzIm) [22]. The specific choice of the diimine ligands is

Dedicated to Prof. Richard Adams at the occasion of his retirement, with warmest wishes for many more happy and healthy years to come.

* Corresponding author.
E-mail address: rainer.winter@uni-konstanz.de (R.F. Winter).

https://doi.org/10.1016/j.jorganchem.2026.124048
Received 26 November 2025; Received in revised form 12 January 2026; Accepted 28 January 2026
Available online 29 January 2026

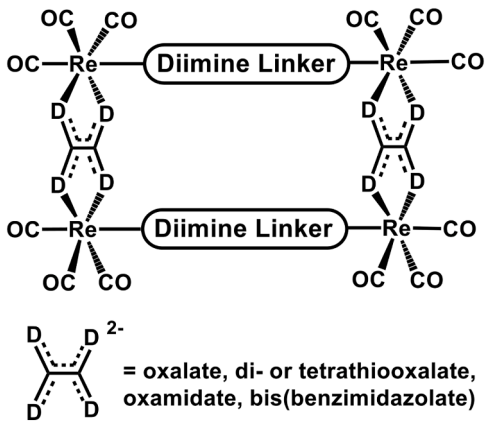

Scheme 1. Generic structure of so-called *Re*-rectangles.

linked to the interesting photophysical properties of core-rigidified derivatives of 4,4′-bipyridine, e. g. such with an EAr_2 group (E = Si, Ge; Ar = Ph, 4-OMePh) [36] as the linkers. The latter compounds are dual fluorescence and phosphorescence emitters, depending on the temperature, thus proving their ability to efficiently populate excited triplet states. On the other hand, the 2,2′-bis(benzimidazolate) linker is known to provide moderately strong electronic coupling in the MV state which can be interrogated and quantified by molecular spectroscopy [22, 30–32]. We here report the successful synthesis and characterization of complexes **2a,b** as well as their mixed-valent and luminescent properties.

2. Results and discussion

Scheme 2 summarizes the synthesis of the new *Re*-rectangles **2a,b**. Complexes **2a,b** were obtained in good yields of 71 % or 78 % after workup by heating equimolar quantities of the dirhenium precursor {*Re*$(CO)_4$}$_2$(BiBzIm) **1** [22] and thieno[2,3-c:5,4-c']dipyridine [24] (**a**) or the newly devised 9-(4-methylthiophenyl)-9H-pyrrolo[2,3-c:5,4-c'] di-pyridine (**b**) in THF for 48 h under reflux conditions. During the course of the reactions, the CO stretching vibrations in the IR spectra change from the four-band pattern of D_{2h} symmetric **1** to a the three- or two-band pattern of *fac*-{*Re*$(CO)_3$} entities, depending on whether or not the E_x and E_y (or, rather A'$_2$ and A'' bands in local C_{2v} symmetry) are individually resolved [37]. This fully agrees with previous observations on *Re*-rectangles [31]. We note a slight, average red-shift of ca. 3 cm^{-1} of all CO bands of **2b** with respect to **2a**, which attests to a higher degree of electron donation from the carbazole-derived ligand **b**.

The purity of the two macrocycles was confirmed by IR and

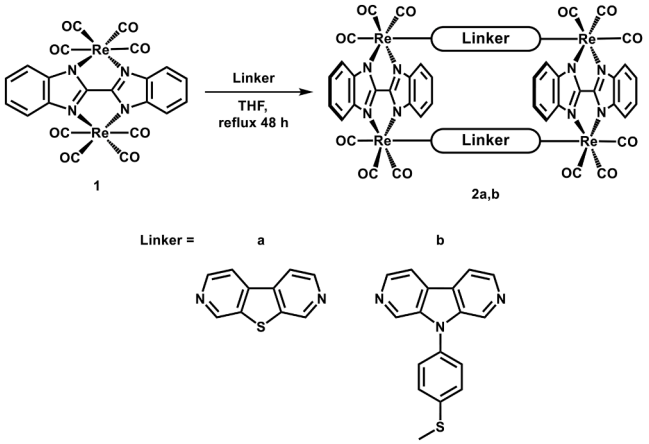

Scheme 2. Synthesis of the rectangular *Re*-metallamacrocycles 2a,b.

multinuclear NMR spectroscopy as well as by high-resolution mass spectrometry. The ^{1}H NMR spectra are shown in Fig. 1, while all other spectra can be found in the Supporting Information. The presence of only one set of resonances for the two wings of the diimine ligands and the absence of any signals for uncoordinated imine donors indicate the cyclic nature of the products. Substitution of a CO ligand at every {*Re*$(CO)_4$} entity of **1** by an imine donor induces a shift of the α- and β-protons of the BibzIm ligand of ca. 0.1 ppm to lower field, whereas the protons at the diimine linker experience a pronounced shift of 0.60 to 0.83 ppm to higher field. One striking difference between complexes **2a, b** is the presence of just one sharp resonance each for the BibzIm α- and β-protons, indicating free rotation of the thienodipyridine linkers around the *Re*-N axes in **2a**. In contrast, there are four separate resonances for BibzIm aryl protons and carbon atoms in **2b** We also note a broadening of the resonance signals for the protons at the appended thioanisyl substituents of the diimine linker at r. t. and their sharpening on increasing the temperature. This indicates that rotation of the diimine linkers in complex **2b** is hindered and that **2b** adopts a preferred orientation where both thioanisyl pendants point to the same side, thereby desymmetrizing the BibzIm ligands at the short edges. A less likely, rarely observed alternative is a structure where the diimine linkers are more or less orthogonal to each other, [31] as was observed in the 4,4′-bipyridine-linked congener by X-ray crystallography. Additional support for such a structural preference comes from DFT calculations, which place the *cisoid* conformer of **2b** at 26 kJ/mol lower energy than the *transoid* structure, but fail to locate a stable conformer with orthogonal orientation of the diimine linkers. The *cisoid* conformer of **2b** also profits from attractive π-stacking interactions between the parallel-aligned thioanisyl pendants (see also Fig. S6.3 of the Supporting Information), which would also explain why their rotation is slowed.

Like similar *Re*-rectangles with π-extended diimine ligands, [22, 30–32] complexes **2a,b** feature four consecutive one-electron reductions in their cyclic and square wave voltammograms (Figure 2; additional voltammograms recorded at different sweep rates are provided in the Supporting Information). Table 1 lists pertinent data. All four waves of **2a** as well as the first two waves of complex **2b** appear to be chemically reversible, at least on the voltammetric timescale. Closer analysis of the third and fourth reductions of **2b** in cyclic voltammetry is hampered by their proximity to the cathodic breakdown limit of the solvent; the corresponding square wave peaks however appear normal. All four redox processes can be assigned to sequential reductions of the diimine linkers by first one and then a second electron. This contrasts with the redox behavior of the free ligands, which can be only reduced once within the accessible potential range of the chosen electrolyte (THF/0.1 M NBu_4PF_6). Bridging coordination to two strongly Lewis-acidic {*Re*$(CO)_3$}$_2$(BiBzIm) entities shifts the first reduction potential of the diimine linkers by 775 or ca. 800 mV to more positive values. This large anodic shift makes also the second ligand reductions accessible [31, 38–40]. The higher electron-richness of ligand **b**, which was already inferred from the lower energies of the CO stretching vibrations in macrocycle **2b**, is internally consistent with the distinctly more negative potentials for each individual redox step of this complex as compared to **2a**, as well as with the ordering of reduction potentials of the free ligands.

Hupp and coworkers have impressively shown that the redox splittings between the first and the second pairs of reduction waves of reducible diimine ligands in *Re*-rectangles, which in the present case amount to 276 mV and 175 mV (**2a**), or 348 mV and 195 mV (**2b**, see Table 1), are not mainly caused by electrostatic repulsion between the negatively charged, cofacially stacked diimine ligands. Rather, they are due to electronic coupling through space between the diimine ligands in the one- and three-electron reduced, mixed-valent (MV) states, where the charges at the two ligands formally differ. They also demonstrated that the magnitude of the redox splitting does not necessarily correspond with the electronic coupling strength, which in turn depends strongly on their stacking distance and π-extension, i. e. the area of ligand π-overlap

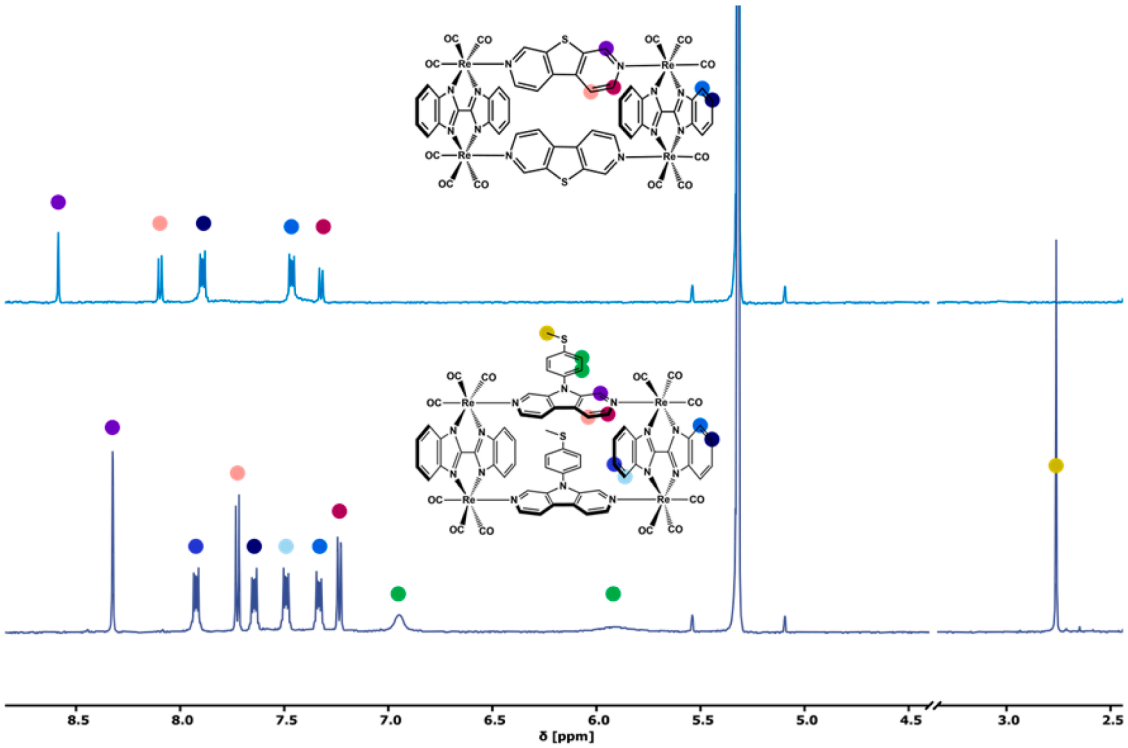

Fig. 1. Relevant parts of the ^{1}H NMR spectra of complexes **2a** (top) and **2b** (bottom) in CD_2Cl_2 at r. t.

Table 1
Electrochemistry Data for the metallamacrocyclic complexes **2a,b** and the corresponding linkers[a].

	$E_{1/2}^{0/-}$	$\Delta E_p^{0/-}$	$E_{1/2}^{-/2-}$	$\Delta E_p^{-/2-}$	$\Delta E_{1/2}^{-/2-}$	$E_{1/2}^{2-/3-}$	$\Delta E_p^{2-/3-}$	$E_{1/2}^{3-/4-}$	$\Delta E_p^{3-/4-}$	$\Delta E_{1/2}^{3-/4-}$
a[b]	−2338	102	-	-		-	-	-	-	
b[b]	−2487	86	-	-		-	-	-	-	
2a	−1563	69	−1839	67	276	−2432	69	−2607	74	175
2b	−1691	76	−2039	80	348	−2746	97	−2941	-	195

[a] All potentials are given in mV (±5 mV) relative to the $Cp_2Fe^{0/+}$ redox standard set as 0 mV in THF/0.1 M $^{n}NBu_4PF_6$ at 293±3 K and at a sweep rate ν of 100 mVs^{-1}.
[b] In DMF/0.1 M $^{n}NBu_4PF_6$ at 293±3 K.

and the extent to which the negative charge(s) spread out [31–32].

As electrochemical redox potential splittings are no faithful reporters of electronic coupling, [41] any reliable assessment of its magnitude requires more indicative results from molecular spectroscopy. Such information can e.g. be gleaned from an analysis of the electronic intervalence charge-transfer (IVCT) excitation. MV compounds with strictly localized valencies, i.e. of Class I according to the classification scheme of Robin and Day, [42] will show no such absorption, whereas it will be present in more strongly coupled MV systems of Class II with partially delocalized valencies and in Class III MV systems with fully delocalized electronic ground states. The latter excitation thus either involves a shift of electron density from the more reduced to the more oxidized site for MV systems of Class II or corresponds to an electronic transition between two electronic states that are both characterized by symmetric charge density distributions (Class III). With increasing degree of electronic coupling, the IVCT transition is generally expected to intensify while the width-at-half-height $\Delta\tilde{\nu}_{1/2}$ will decrease.

In-depth studies on MV anions of *Re*-rectangles have shown a clear correlation between the electronic coupling strength and the stacking distance of the diimine linkers. Thus, the one-electron reduced MV forms of *Re*-rectangles with ethoxido or phenylthiolato lateral linkers and short distances of ca. 3.6 Å between the diimine ligands exhibit fully delocalized behavior,[30] corresponding to MV compounds of Class III, while those with longer 2,2′-bis(benzimidazolate) spacers and a distance of ca. 5.3 Å between the diimines belong to Class II or the weakly delocalized Class II/I limit with H_{ab} values in the range of 400 to 1000 cm^{-1} and α values of 0.07 to 0.20. As α measures the charge already transferred from the more electron-rich to the less electron-rich redox site in the electronic ground state of an MV system, these values correspond with charge-density distributions of 93:7 or 80:20 between the diimine ligands [31]. When combined with the same {*Re*(CO)$_3$}$_2$(BiBzIm) template, bending at the ethynyl connections allows the central porphyrin units of the more flexible [5,15-bis(4-ethynylpyridyl) porphyrinato]zinc diimine linker to approach as closely as 3.4 Å, [32, 43] thereby allowing for strong interligand electronic coupling in the MV state. This renders the associated 1− anion a Class II/III borderline system whose degree of charge equilibration depends on the solvent, i.e. the rate and extent to which the solvent shell stabilizes an asymmetric or a symmetric electron density distribution and the rate at which it can adapt to temporal fluctuations of the latter [32]. Owing to their very negative reduction potentials and inherent high reactivity, studies on the likewise mixed-valent trianions are more scarce. It however seems that they are considerably less strongly coupled than the corresponding singly reduced forms, which has been attributed to increased stacking distances due to enhanced electrostatic repulsion in the higher charged 3− state [21,31].

The extraction of the electronic coupling parameter H_{ab} or the delocalization parameter α from the IVCT bands in the Class II régime requires information on the effective charge-transfer distance R_{ab}, which is difficult to obtain experimentally [44–45]. The latter can be

considerably smaller than the spatial (or geometric) separation between the redox sites. The direct correlation between the CO stretching vibrations of a $\{M(CO)_n\}$ entity with the local electron density at the metal ion to which the CO ligands are bonded provides a highly convenient tool to analyze the mixed-valent forms of metal carbonyl complexes, even in a quantitative manner, that does not require such information [46–47]. In the present case of *Re*-rectangles with four $\{Re(CO)_3\}$ moieties of local C_s or C_{2v} symmetry, the unique A'$_1$ mode can be used as a probe of intrinsic charge (de)localization on the vibrational picosecond timescale. Only one such band is expected, if, in the MV state, the uninegative charge is evenly spread over both diimine linkers, whereas it will split into two separate bands, if the charges on the diimine ligands differ.

With this in mind, we sought to spectroscopically characterize the various reduced forms of complexes **2a,b**. To these ends we resorted to IR and UV/vis/NIR spectroelectrochemistry (NIR = near infrared), where the corresponding redox species are generated in situ at the electrode surface of an optically transparent thin-layer electrolysis cell [48]. During these investigations the three- and four-electron reduced forms turned out to be too unstable on the longer timescales of electrolysis to allow us to access them. This restricts our discussion to the MV one-electron reduced anions and the bordering isovalent neutral and dianionic forms.

Fig. 3 shows the changes in the IR as well as the IR/NIR regions for complex **2b**; those for **2a** can be found in the Supporting Information. Relevant data are compiled in Table 2. During twofold reduction to the dianions, the A'$_1$ band of **2a,b** shifts from 2024 to 2006 or 2009 cm^{-1}, whereas the initially non-degenerate A'$_2$ and A'' bands combine to a single, broadened band, now likewise located at ca. 20 cm^{-1} lower average energy. The small magnitude of the overall CO band shifts clearly characterizes these redox processes as ligand based, as was found in the previous studies [30–32]. Revealingly, the one-electron reduced monoanions $\mathbf{2a}^{\mathbf{1}-}$, $\mathbf{2b}^{\mathbf{1}-}$ feature *two* A'$_1$ bands, yet at shifted positions with respect to both, the neutral and the dianionic redox states. Such behavior is typical of MV compounds of Class II with only partially delocalized valencies and intrinsically different electron densities at the individual redox sites.

Geiger and coworkers have shown that the relative CO band shifts of a MV species can be used to calculate the charge density distribution parameter $\Delta\rho$ as a quantitative measure of electronic (a) symmetry between the individual redox sites [46–47]. The parameter $\Delta\rho$ is defined in Eq. (1), where $\tilde{\nu}_{ox}$ and $\tilde{\nu}_{red}$ pertain here to the energy of the CO stretch in the neutral and the direduced state, and where $\tilde{\nu}_{ox(MV)}$ and $\tilde{\nu}_{red(MV)}$ denote the wavenumber of the CO band at the higher or the lower energy in the MV state, as is schematically shown in Fig. 4.

$$\Delta\rho = \frac{(\tilde{\nu}_{ox} - \tilde{\nu}_{ox(MV)}) + (\tilde{\nu}_{red(MV)} - \tilde{\nu}_{red})}{2(\tilde{\nu}_{ox} - \tilde{\nu}_{red})} = \frac{\Delta\tilde{\nu}_{ox} + \Delta\tilde{\nu}_{red}}{2(\tilde{\nu}_{ox} - \tilde{\nu}_{red})} \quad (1)$$

With the values of Table 2, the $\Delta\rho$ psarameter of $\mathbf{2a}^{\mathbf{1}-}$ has a value of 0.23, while that of $\mathbf{2b}^{\mathbf{1}-}$ is slightly larger at 0.28. These values characterize the MV anions as moderately strongly coupled mixed-valent systems of Class II where the one diimine ligand carries ca. 75 %, and the other ca. 25 % of the uninegative charge.

Quantum chemical calculations on molecular rectangles **2a,b** provide further tokens of electronic coupling between the diimine ligands in the MV state. One such piece of evidence comes from the energy splitting of 0.05 eV (405 cm^{-1}) or 0.06 eV (485 cm^{-1}) between the orbitals LUMO and LUMO+1 (LUMO = energetically lowest-lying unoccupied molecular orbital), which represent in-phase (LUMO) and out-of-phase combinations (LUMO+1) of the same diimine π* orbitals (Fig. 5). In the absence of electronic coupling, these MOs would be energetically degenerate [30–31,49]. Comparison of the DFT-optimized structures of the neutral and one-electron reduced forms suggests that through-space interactions between the diimine ligands increase on one-electron reduction (see the Supporting Information for their geometry-optimized structures). Thus, the spatial separation between the centroids of the inner five-membered rings decreases from 5.108 Å (**2a**) or 5.198 Å (**2b**) to 4.486 Å or 4.538 Å in the corresponding singly reduced anion. This is accompanied by a decrease of the average angles *Re*···*Re*-N from 83.5° to 82.8°, or from 83.9° to 82.9°, as the diimine ligands bend further inward.

As is expected for electronically coupled MV systems, the singly reduced anions of complexes **2a,b** feature a characteristic IVCT band in the NIR with a maximum at 4450 cm^{-1} (2250 nm, $\mathbf{2a}^{\mathbf{1}-}$) or 4305 cm^{-1} (2320 nm, $\mathbf{2b}^{\mathbf{1}-}$, see Fig. 3), which closely resemble those of the MV forms of other *Re*-rectangles with $\{Re(CO)_3\}_2$(BiBzIm) edges [31]. This absorption is specific to the 1− redox state. It forms during the first reduction and then bleaches out during further reduction to the dianion, while other bands that involve reduced diimine ligands continue to grow in intensity (see also Fig. 7). Our IR data indicates that both MV anions belong to Class II with partially (de)localized valencies. In this limit, and under the assumption that the system is adequately described by a two-level model, the electronic coupling parameter H_{ab} can be

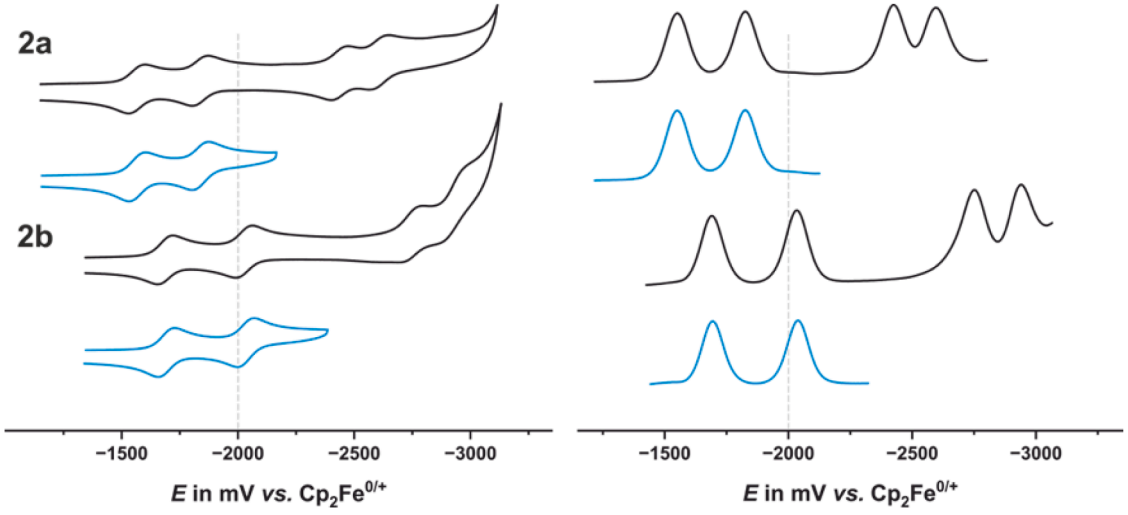

Fig. 2. Cyclic (left) and square wave voltammograms (right) of metallamacrocycles **2a** (top) and **2b** (bottom) with scanning over exclusively the first two (blue lines) or all four redox processes that fall within the accessible solvent limit (black lines). The grey dotted vertical bars are intended as guides to the eye. The measurements were performed in THF/0.1 M $^{n}Bu_4NPF_6$ at a sweep rate *v* of 100 mVs^{-1}, or with a step height of 4 mV, a step amplitude of 25 mV and a frequency of 25 Hz for square wave voltammetry at room temperature (r. t.). The potential scale is relative to the ferrocene/ferrocenium redox couple, which is set as 0 mV.

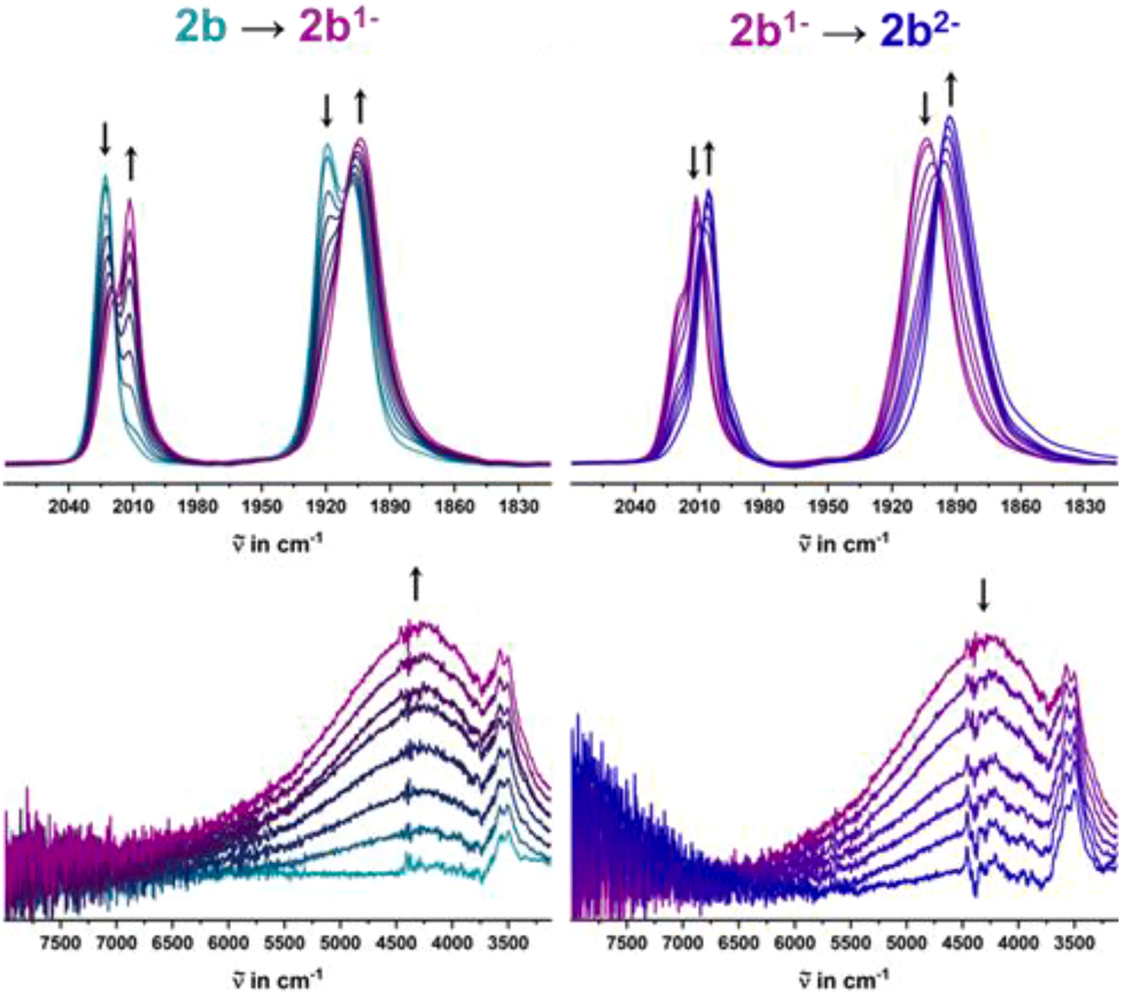

Fig. 3. Changes in the IR spectra of complex **2b** in the energy range of the carbonyl ligand CO stretching vibrations (top) and in the NIR range of the IVCT transition (bottom) during the first (left) and the second (right) reduction in THF/0.1 M $^{n}NBu_4PF_6$ as the supporting electrolyte.

calculated according to Hush [50–51] from the energy $\tilde{\nu}_{max}$, the extinction coefficient ε_{max}, and the width at half-height $\Delta\tilde{\nu}_{1/2}$ of the IVCT band, and the effective charge transfer distance R_{ab}, as given in Eq. (2). Relevant data are collected in Table 3.

$$H_{ab} = \frac{0.0206}{R_{ab}}\sqrt{\tilde{\nu}_{max}\cdot\Delta\tilde{\nu}_{1/2}\cdot\varepsilon_{max}} \quad (2)$$

It was shown that the geometric stacking distance between diimine ligands R_{stack} tends to overestimate the effective charge transfer distance so that H_{ab} values derived from such an approximation represent a lower limit [31–32]. In the present case, setting R_{ab} as the vertical distance between the centroids of the ligands as retrieved from DFT modeling provides a value H_{ab} of 330 cm^{-1} for $\mathbf{2a}^{\mathbf{1}-}$, and one of 640 cm^{-1} for $\mathbf{2b}^{\mathbf{1}-}$. These values resemble those for the pyrazine- (H_{ab} = 400 cm^{-1}) and the 2,7-diazapyrene-bridged tetrarhenium complexes (H_{ab} = 600 cm^{-1}) with the same {$Re_2(CO)_6$(BiBzIm)} building blocks [31]. In both cases, the experimental IVCT band width at half-height $\Delta\tilde{\nu}_{1/2}$ is considerably smaller than that calculated using Hush's expression for a Class II MV species, $\Delta\tilde{\nu}_{1/2,theor}$s, in Eq. (3) [50].

$$\Delta\tilde{\nu}_{1/2} = \sqrt{16\ln(2)k_B T\tilde{\nu}_{max}} = \Delta\tilde{\nu}_{1/2,theor} = \sqrt{2310\tilde{\nu}_{max}} \quad (3)$$

The ratio $H_{ab}/\tilde{\nu}_{max}$ of the IVCT band is known as Hush's delocalization parameter α and represents the charge imbalance of the redox centers in the MV state. It hence assumes a value of 0.50 for a completely delocalized MV system of Class III, but becomes smaller for a Class II system [31]. Values of H_{ab} and α of MV complexes $\mathbf{2a,b}^{\mathbf{1}-}$ are in the same range as those for their congeners with 4,4′-bipyridine (H_{ab} = 1000 cm^{-1}, α = 0.20), 3,6-bis(4-pyridyl)-1,2,4,5-tetrazine (H_{ab} = 800 cm^{-1}, α = 0.12), 2,7-diazapyrene (H_{ab} = 600 cm^{-1}, α = 0.14) or pyrazine (H_{ab} = 400 cm^{-1}, α = 0.07) as the diimine ligands [31]. We note that the α values of $\mathbf{2a,b}^{\mathbf{1}-}$ are only about half as large as their charge distribution parameters Δρ, although both, α and Δρ, represent the charge imbalance of the redox centers in the MV state. It thus seems that the geometric separation of the diimine ligands overestimates the effective charge transfer distance by about the same margin. This suggests that IR spectroscopy, which does not require such simplifying assumptions, is a more reliable tool for quantitatively assessing the extent of electronic communication in MV states in such systems than analyses of the IVCT band.

UV/vis spectra of the neutral complexes **2a,b** are shown in Fig. 6. Both compounds absorb strongly in the UV, exhibiting vibrational structuring of their electronic absorption bands with resolved peaks at 321, 330, 339, 350, 359 and 373 nm. Identical bands were observed for other *Re*-rectangles with the {$Re(CO)_3$}$_2$(BiBzIm) motif so that they can be assigned to intraligand π→π* transitions within the common BiBzIm linker [30–31,49]. The higher extinction coefficient of **2b** suggests that in this case the band is augmented by a π→π* excitation within the diimine ligand, which is confirmed by our quantum chemical calculations. We note that the HOMO and HOMO−1, which are both localized on the BiBzIm ligands, are energetically degenerate due to the large distances spanned by the diimine linkers, contrary to what is observed

Table 2
IR, UV/vis/NIR and photoluminescence data for complexes **2a** and **2b**.

	$\tilde{\nu}_{CO}$[a]	λ_{max} (ε_{max})[b,c]	λ_{Em}[b]	τ_{ph}[d]	Φ_{ph}[d]
2a	2024, 1919, 1909	339 (29.1), 350 (31.9), 359 (27.7), 372 (24.6)	512[e]	40 [78 %], 84 [22 %][a]	1.1
			638[f]	0.34 [64 %], 2.3 [36 %]	62
2a^{1-}	2021, 2013, 1906	338 (27.8), 349 (31.2), 358 (27.5), 371 (26.2), 408 (9.1), 653 (4.0), 2250 (1.10)	-	-	n. det.
2a^{2-}	2009, 1896	337 (28.5), 348 (32.6), 357 (29.8), 371 (30.5), 398 (16.7), 633 (8.1)	-	-	n. det.
2b	2024, 1919, 1908	339 (38.7), 350 (41.0), 360 (36.0), 373 (34.1)	520, 550[e]	137 [55 %], 345 [45 %][a]	2.0
			600[f]	0.31 [92 %], 0.79 [8 %]	91
2b^{1-}	2019, 2011, 1903	337 (37.1), 349 (41.3), 357 (37.8), 370 (38.8), 657 (5.7), 2320 (2.76)	-	-	n. det.
2b^{2-}	2006, 1893	337 (38.9), 348 (42.7), 357 (38.7), 371 (40.0), 650 (6.2)	-	-	n. det.

[a] $\tilde{\nu}_{CO}$ in cm^{-1} in THF/0.1 M NBu_4PF_6.
[b] λ in nm.
[c] ε_{max} in $\times 10^3$ $M^{-1}cm^{-1}$.
[d] τ_{ph} in μs; relative contributions in %.
[e] In 2-MeTHF at 77 K. [f] In THF at room temperature (r. t.).

for the diimine-based LUMO and LUMO+1 (vide supra). The spectra of both complexes also exhibit a distinct shoulder that extends well into the visible régime, down to ca. 450 nm, endowing their solutions with a yellow to yellow-orange coloration. Our TD-DFT calculations predict several electronic excitations in this energy range that emanate from the HOMO−2 or lower-lying occupied MOs, all with dominant {*Re*(CO)$_3$} character and only small contributions from the dianionic BiBzIm ligands. As the latter excitations target the orbitals LUMO and LUMO+1, they have *Re*-to-diimine charge-transfer (i.e. MLCT) character. This agrees with previous assignments [18,22,30,52].

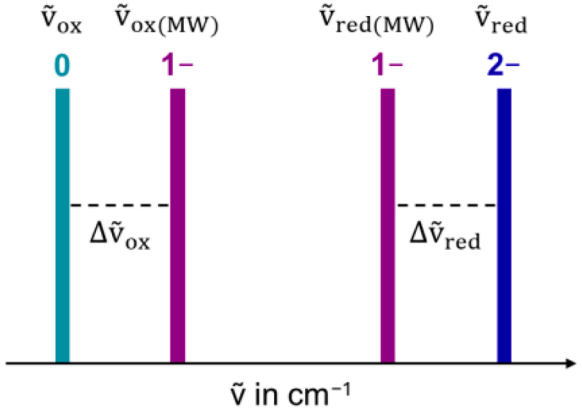

Fig. 4. Schematic representation of the CO band positions and shifts used to define the charge density distribution parameter $\Delta\rho$ according to Atwood and Geiger [46–47].

The most significant change in the UV/vis spectra during stepwise reduction is the appearance of a new absorption, which is initially located at ca. 650–660 nm and intensifies upon the second reduction with a slight, concomitant blue shift (see Fig. 7 and Table 2). Such bands were previously assigned as π→π* excitations within the one-electron reduced diimine ligands [21,31]. According to our TD-DFT calculations, they are rather described as LMCT excitations that shift electron density from the reduced ligand(s) to the {*Re*(CO)$_3$} fragments. In the case of **2b**$^{1-}$, this band is augmented by intraligand CT from the carbazole core entity to the outer *N*-thioanisyl substituents of the diimine linkers. TD-DFT calculated spectra and the corresponding electron density difference maps can be viewed in the Supporting Information. The slight blue-shift of this band during the second reduction can be regarded as an indication for partial charge equilibration between the *Re* entities at the two short sides of the *Re*-rectangles that is passed on from one side to the other by the bridging BiBzIm and the π-stacked diimine ligands. Both effects contribute to an energetic destabilization of the *Re* acceptor orbitals as the overall negative charge increases.

Like several other *Re*-rectangles of this general type, [17–29] complexes **2a,b** emit from an excited ^{3}MLCT state at room temperature and as frozen solutions in 2-MeTHF at 77 K. The phosphorescent nature of the emission is indicated by the broad emission envelopes (see the right-hand panels of Fig. 8), large Stokes shifts and long emission lifetimes of several hundred nanoseconds (Table 2) for rigorously deaerated solutions (three freeze-pump-thaw cycles). The emission is in the deep red (**2a**) or orange red (**2b**) with lifetimes $\tau_1 = 0.34$ μs and $\tau_2 = 2.3$ μs for **2a**, and $\tau_1 = 0.32$ μs and $\tau_2 = 0.79$ μs for **2b**, and with quantum yields of 1.1 % for **2a** and 2.0 % for **2b** Cooling to 77 K changes the emission color to yellow-green, now peaking at 512 nm (see the upper left panel of Fig. 8). Such rigidochromism [18,53] of emissive *Re*-rectangles has been observed on other occasions. It points to significant structural reorganization in the photoexcited ^{3}LMCT state, which is blocked in a rigidly frozen matrix, so that the emission occurs from a higher-energy structure that resembles the electronic ground state more closely. Under cryogenic conditions, the radiative lifetimes of **2a** increase to $\tau_1 = 40$ μs and $\tau_2 = 84$ μs while the quantum yield assumes a value of 62 %. **2b** emits at a similar wavelength but features a partially resolved shoulder at 550 nm (see the bottom left panel of Fig. 8). Its quantum yield of 91 % and radiative lifetimes of the bimodal emission ($\tau_1 = 137$ μs, $\tau_2 = 345$ μs) are even higher and longer compared to those of **2a**.

The quantum yields of **2a,b** are the largest for this class of compounds that we are aware of. They are next rivaled by those of 15.7 % and 31.9 % reported for similar macrocycles with 1,4-dioxido-9,10-

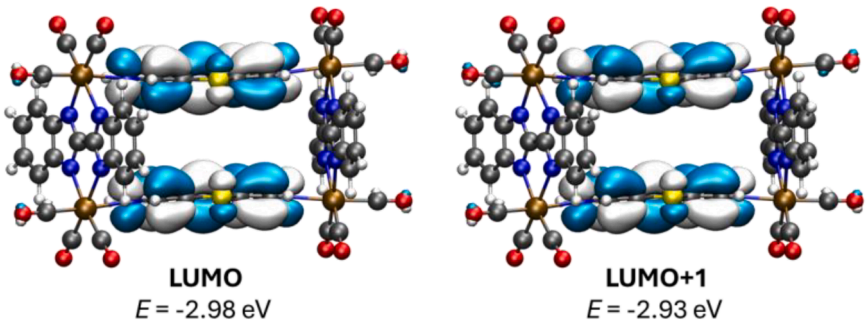

Fig. 5. DFT-computed contour diagrams of the LUMO and LUMO+1 of **2a**, representing the in- and out-of-phase combinations of the same diimine π* orbitals, with their energies.

Table 3
Data for the IVCT band, the theoretical width at half-height $\Delta\tilde{\nu}_{1/2,\text{theor}}$, and the derived electronic coupling parameter H_{ab} for $\mathbf{2a}^{1-}$ and $\mathbf{2b}^{1-}$.

	$\tilde{\nu}_{max}$ (cm^{-1})	ε_{max} ($M^{-1}\cdot cm^{-1}$)	R_{ab} (Å)	H_{ab} (cm^{-1})	α	$\Delta\tilde{\nu}_{1/2}(cm^{-1})$	$\Delta\tilde{\nu}_{1/2,theor}(cm^{-1})$
$\mathbf{2a}^{1-}$	4450	1100	4.486	330	0.07	1064	3200
$\mathbf{2b}^{1-}$	4305	2760	4.538	640	0.15	1664	3150

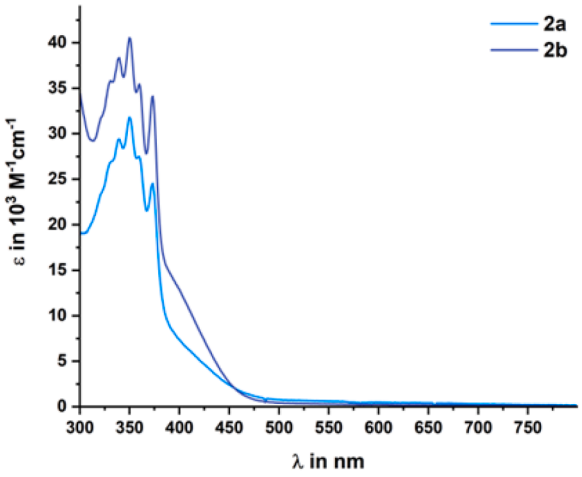

Fig. 6. UV/Vis absorption spectra of complexes **2a** (sea blue) und **2b** (dark blue) in THF at r. t.

anthraquinones as lateral ligands and 4,4′-bipyridine as the diimine linkers at 77 K (no data at r. t. given) [21]. Quantum yields of other metallamacrocyclic *Re* complexes that were reported in the literature are in the range of 0.039 to 0.22 % [25,28] at room temperature, including such with {$Re(CO)_3X$} (X = Cl, Br) corners and pyrazine, 4,4′-bipyridine, [20] bis(4-pyridyl)ethynylene, 1,4-bis(4-ethynylpyridyl) buta-1,4-diyne, [27] *trans*-bis(4-pyridyl)ethene, 2,5-bis(4-pyridylthiophene), [27] 1,4-bis(4-pyridylethynyl)-benzene, [27,29] 1,4-bis(4′-pyridylethynyl)naphthalene, or 1,4-bis(4′-pyridylethynyl)anthracene [29] as the diimine linkers. We attribute the enhanced photophysical properties of complexes **1** and **2** to the high rigidity of the diimine ligands used herein, which prevents radiationless decay by rotational motions within the linkers, and the inherent propensity of core-rigidified 4,4′-bipyridines to undergo ISC [36]. Admission of dioxygen partially quenches the emission and shortens the emissive lifetimes to $\tau_1 = 5.5$ ns and $\tau_2 = 64$ ns (**2a**), or to 1.8 ns (**2b**). Emission spectra in the presence and absence of oxygen and plots showing the temporal emission decay with the fitted lifetimes can be found in the Supporting Information.

We finally mused that the Au-coordinating thioether functionalities embedded within (**2a**) or appended to the diimine ligands (**2b**) render metallamacrocycles **2a,b** amenable to molecular conductance studies with an STM-based break-junction setup [54–58]. Macrocyclic structures are particularly attractive subjects for such studies, because theory has predicted that molecules with two or more parallel conduction strands may exhibit enhanced conductivities compared to two monofunctional wires of identical composition [59]. To date, only few attempts have been made to experimentally verify this intriguing concept, [58] with the 1.6- to 2.8-fold enhancement of molecular conductivity in 2,11-dithia[3,3]paracyclophane motifs as the most impressive result [60]. Unfortunately, repeated cycles of forming and breaking nanosize Au···Au contacts with solutions of **2a,b** in 1,2,4-trichlorobenzene with more than 5000 individual repetitions did not provide a significant number of defined traces that could be associated with individual molecules that bridge between the Au tip and substrate. We attribute this failure to the favored *cisoid* arrangement of the diimine ligands and the binding of both anchoring groups to the Au substrate. This seems to decrease the probability of junction formation to below a statistically relevant level.

3. Summary and conclusions

We herein present our results on two new metallamacrocycles based on {$Re(CO)_3$}$_2$(BiBzIm) edges with core-rigidified thieno[2,3-c:5,4-c'] dipyridine (complex **2a**) or 9-(4-methylthiophenyl)-9H-pyrrolo[2,3-c:5,4-c']dipyridine (complex **2b**) diimine linkers. One key aspect of this work is the use of IR spectroelectrochemistry to quantify the extent of charge (de)localization in their mixed-valent, one-electron reduced forms, where the unique A'$_1$ $Re(CO)_3$ mode serves as an indicator of the charge state of each of the bridged {*Re*}-diimine-{*Re*} vertices. The relative CO band shifts with respect to the bordering isovalent states provide values of the Geiger charge distribution parameter $\Delta\rho$ of 0.23 for $\mathbf{2a}^{1-}$ and of 0.28 for $\mathbf{2b}^{1-}$. The values of $\Delta\rho$ are nearly twice as large as those of Hush's delocalization parameter α derived from IVCT band analysis. On the other hand, the present data of the electronic coupling strength H_{ab} and α are in the same range as for similar *Re*-rectangles with

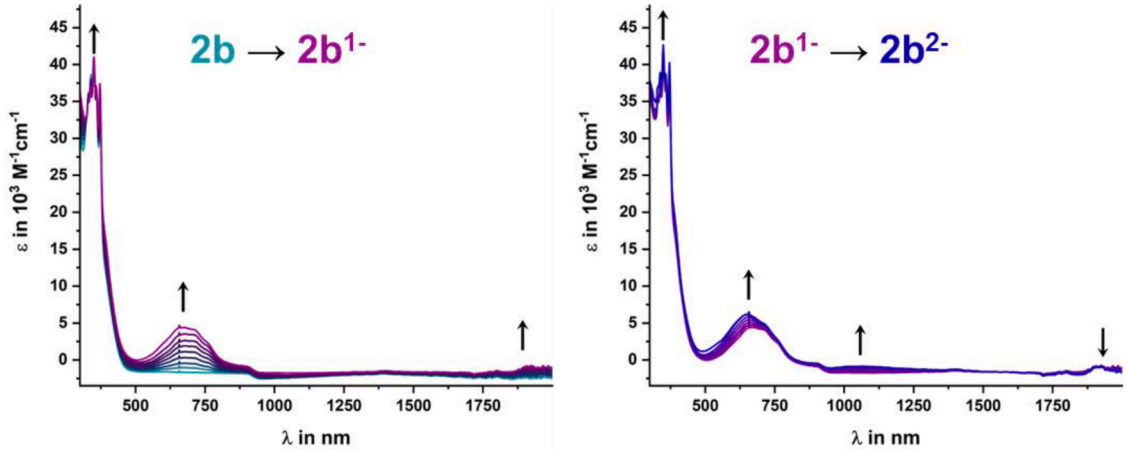

Fig. 7. Changes in the UV/vis/NIR spectra of complex **2b** during the first (left) and the second (right) reduction, as measured with a spectroelectrochemical thin-layer cell at r. t., and in THF/0.1 M ^{n}NBu$_4$PF$_6$ as the supporting electrolyte.

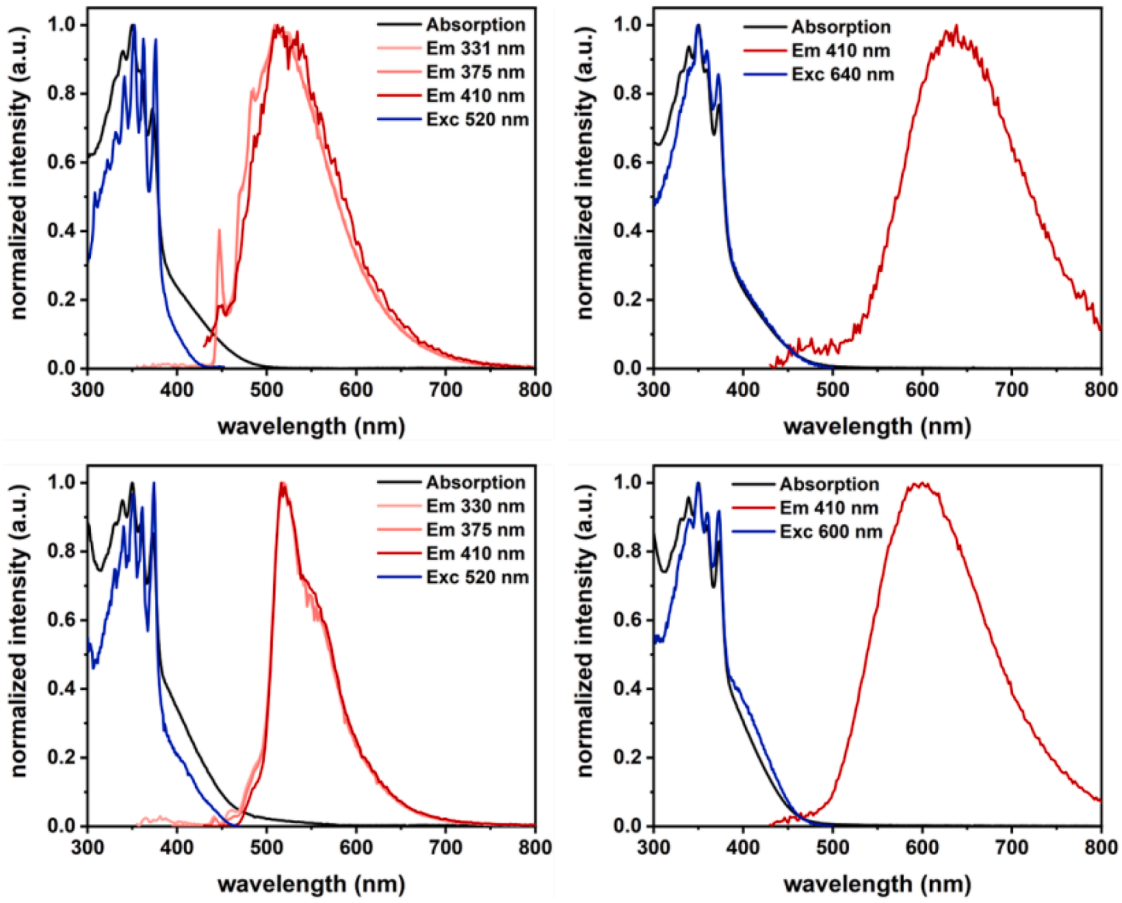

Fig. 8. Emission spectra of the metallamacrocycles **2a** (top panels) and **2b** (bottom panels) at 77 K in 2-MeTHF (left panels) and at room temperature in degassed THF (right panels). Absorption spectra are shown as black lines, emission spectra as red lines, and excitation spectra as blue lines with the excitation and probe wavelengths given in the legend.

the same {*Re*(CO)$_3$}$_2$(BiBzIm) edges and hence grossly similar lateral stacking distances between the charge-bearing diimine ligands [31]. It thus seems that the stacking distance between the diimine ligands overestimates the effective charge-transfer distance R_{ab} by about the same margin.

Another remarkable asset of the present compounds are the high quantum yields for their phosphorescence emission, both at room temperature (Φ_{Ph} = 1.1 % and 2.0 %) and at cryogenic temperatures in the frozen state (Φ_{Ph} = 62 % and 91 %). They seem to be the highest values reported to date for this class of compounds. We attribute their enhanced emission performance to the rigidification of the 4,4′-bipyridine skeleton by the heteroatom bridge, which diminishes radiationless decay through the activation of torsional modes within the diimine linkers.

Attempts to employ complexes **2a,b** with their thioether-modified diimine ligands as molecular conduits in STM-based break-junction experiments remained however unsuccessful. We attribute this to their *cisoid* arrangement and preferred simultaneous anchoring of both thioether functionalities of a macrocycle to the Au substrate.

4. Experimental section

4.1. General methods

All syntheses were performed under inert gas atmosphere using standard Schlenk techniques with dry, distilled, and nitrogen-saturated solvents. All reagents were purchased from commercial sources and were used without further purification. ^{1}H NMR (600 MHz) and ^{13}C NMR (151 MHz) spectra were recorded on a Bruker Avance III 600 spectrometer. Thieno[2,3-c:5,4-c']dipyridine [24] and {Re$_2$(CO)$_6$}$_2$(BiBzIm)] [22] were prepared according to established literature protocols.

4.1.1. Electrochemical and spectroelectrochemical measurements

Voltammetric investigations of the complexes were carried out using a cylindrical, vacuum-tight single-compartment cell. A silver wire (as a pseudoreference electrode) and a coiled platinum wire (as a counter electrode) are attached to opposite sides of the cell using quick-fit connectors. A glassy carbon electrode MF-2012 from the manufacturer BASi (Bioanalytical Systems, Inc., ∅ 3 mm) was used as the working electrode. It was inserted into the analyte solution via the top port with a quick-fit screw. Before each set of measurements, the working electrode was polished with diamond pastes from the manufacturer Buehler GmbH (MetaDi II with a grain size of 1 μm and 0.25 μm) using MetaDi fluid as a lubricant. The voltammetric measurements were performed on a computer-controlled potentiostat Epsilon from BASi. ^{n}Bu$_4$N$^+$ PF$_6^-$ (0.1 M) was used as the electrolyte for the measurements in THF and DMF. The amount of solvent used for each measurement was approximately 7 mL. Referencing was performed by adding an equimolar amount of decamethylferrocene ($E_{1/2}$ (Cp*$_2$Fe$^{+/0}$) = −540 mV vs. Cp$_2$Fe$^{0/+}$). All measurements were performed under an argon atmosphere.

The spectroelectrochemical measurements were performed in an OTTLE cell (OTTLE = optically transparent thin-layer electrochemical cell), which was custom-built according to the design of Hartl et al. [48] The cell consists of three electrodes placed between CaF$_2$ windows. A platinum mesh electrode serves as the working and counter electrodes, and a thin silver plate coated with silver chloride as the reference electrode. The electrodes are sealed into a polypropylene spacer. A Wenking Pos 2 potentiostat from Intelligent Controls GmbH was used to

control the applied potential. $^{n}Bu_4N^+$ PF_6^- (0.1 M in THF as the solvent) was used as the supporting electrolyte. The potential was incrementally increased with continuous monitoring of IR/NIR or UV/vis/NIR spectra. FT-IR spectra were recorded using a Bruker Tensor II FT-IR spectrometer. UV/vis/NIR spectra were recorded using a fiber optic diode array spectrometer TIDAS, which combines MCS UV/vis and PGS NIR instruments from j&m Analytik AG.

4.1.2. Quantum mechanical calculations

The electronic ground-state structures of the complexes were determined using density functional theory (DFT) with the Gaussian 16 software package [61]. The geometry optimization and subsequent vibration analysis were performed taking the solvent into account, with solvent effects described by the polarizable continuum model (PCM) using standard parameters for tetrahydrofuran [62]. For all atoms, 6–31G(d) polarized double-ζ basis sets were used together with the exchange and correlation functional (PBE0) of Perdew, Burke and Ernzerhof [63]. The GaussSum software package was used to analyze the results [64]. Computational results were visualized using the Avogadro software package [65]. Graphical representations of molecular orbitals were created using GNU Parallel and visualized with the vmd program package [66] in combination with POV-Ray [67].

4.1.3. Photoluminescence spectroscopy

The luminescence spectra and lifetimes of solutions of the respective compound in 2-MeTHF (77 K) or in THF (r. t.) were measured on a PicoQuant FluoTime 300 spectrometer. Absolute quantum yields were determined with an integrating sphere within the FluoTime 300 spectrometer. Solutions were degassed through three cycles of freeze-pump-thaw.

4.2. Synthesis

3,3′-Dibromo-4,4′-bipyridine [68]

Di^{iso}propylamine (2.3 mL, 1.69 g, 16.7 mmol, 1.0 eq.) was dissolved in THF (40 mL) and subsequently cooled to −78 °C. ^{n}BuLi (2.5 M, 6.0 mL, 0.97 g, 15.0 mmol, 0.9 eq.) was added dropwise. The colorless reaction solution was stirred for one hour at −78 °C. After cooling the reaction solution to −98 °C, 3-bromopyridine (1.31 g, 15.2 mmol, 1.0 eq.) was added dropwise, forming an orange suspension. The resulting reaction mixture was stirred for one hour at −98 °C. $CuCl_2$ (4.85 g, 36.1 mmol, 2.4 eq.) was added in one portion. The resulting reaction mixture was stirred for a further 20 min in the cooling bath. Then, the cooling bath was removed, and the reaction mixture was stirred for 48 h at room temperature. The solvent was removed in vacuo, and the brown residue was mixed with a solution of H_2O (35 mL), NH_3 (25 %, 15 mL) and saturated aqueous NH_4Cl solution (15 mL). The blue solution was extracted with CH_2Cl_2 (3 × 70 mL). The combined organic phases were washed with H_2O (3 × 100 mL), dried over $MgSO_4$, and the solvents were removed in vacuo. The residue was purified by column chromatography (PE:EtOAc (2:1, v/v)). 3,3′-Dibromo-4,4′-bipyridine was obtained as a beige solid (0.91 g, 2.9 mmol, 19 %). The obtained ^{1}H NMR spectrum matches with data in the literature [68].

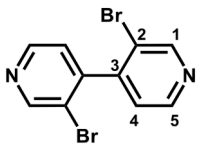

^{1H}NMR (400 MHz, C_6D_6): δ in ppm = 8.88 (br s, 2H, $H_{(1)}$), 8.64 (d, 2H, $^3J_{H,H}$ = 4.9 Hz, $H_{(4)}$), 7.18 (d, 2H, $^3J_{H,H}$ = 4.9 Hz, $H_{(5)}$).

Thieno[2,3-c:5,4-c']dipyridine (**a**) [24]

3,3′-Dibromo-4,4′-bipyridine (500.0 mg, 1.59 mmol, 1.0 eq.) was dissolved in THF (50 mL) and subsequently cooled to −84 °C. ^{n}BuLi (2.5 M, 1.3 mL, 0.21 g, 3.34 mmol, 2.1 eq.) was added dropwise, turning the colorless solution red. The resulting reaction solution was stirred for one hour at −78 °C. S_2Cl_2 (1.3 mL, 0.23 g, 1.67 mmol, 1.05 eq.) was slowly added and the yellow solution was allowed to warm to room temperature and stirred overnight. The solvent was removed in vacuo, and a solution of H_2O (35 mL), NH_3 (25 %, 15 mL) and saturated aqueous NH_4Cl solution (15 mL) were added. The mixture was extracted with CH_2Cl_2 (3 × 50 mL). The combined organic phases were washed with H_2O (3 × 100 mL), dried over Na_2SO_4, and the solvents were removed in vacuo. The residue was purified by column chromatography (PE:EtOAC (1:1, *v/v*) to EtOAc (100 %)). Thieno[2,3-c:5,4-c']dipyridine was obtained as a pale yellow solid (82.0 mg, 1.59 mmol, 27 %). The obtained ^{1}H NMR spectrum agrees with literature data [24].

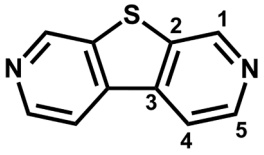

^{1}H NMR (400 MHz, C_6D_6): δ in ppm = 9.29 (d, 2H, $^4J_{H,H}$ = 0.8 Hz, $H_{(1)}$), 8.75 (d, 2H, $^3J_{H,H}$ = 5.4 Hz, $H_{(4)}$), 8.12 (dd, 2H, $^3J_{H,H}$ = 5.4 Hz, $^4J_{H,H}$ = 0.8 Hz, $H_{(5)}$).

9-(4-Methylthiophenyl)-9H-pyrrolo[2,3-c:5,4-c']dipyridine (**b**)

3,3′-Dibromo-4,4′-bipyridine (0.90 mg, 2.87 mmol, 1.1 eq.), 4-methylthioaniline (0.3 mL, 0.36 g, 2.61 mmol, 1.0 eq.), $Pd_2(dba)_3$ (0.24 g, 0.26 mmol, 0.1 eq.), XPhos (0.38 g, 0.78 mmol, 0.3 eq.) and NaO^{t}Bu (0.77 mg, 7.82 mmol, 3.0 eq.) were dissolved in toluene (40 mL). The reaction mixture was stirred for 24 h at 100 °C. After cooling the mixture to room temperature, the reaction mixture was filtered through a silica plug. The solvent was removed in vacuo. 9-(4-Methylthiophenyl)-9H-pyrrolo[2,3-c:5,4-c']dipyridine was obtained as a white solid (0.50 g, 1.73 mmol, 66 %).

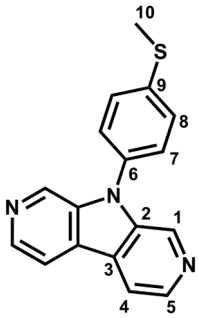

^{1}H NMR (400 MHz, $CDCl_3$): δ in ppm = 8.92 (br s, 2H, $H_{(1)}$), 8.57 (d, 2H, $^3J_{H,H}$ = 5.3 Hz, $H_{(5)}$), 8.03 (d, 2H, $^3J_{H,H}$ = 5.3 Hz, $H_{(4)}$), 7.49 (br s, 4H, $H_{(7)}$, $H_{(8)}$), 2.57 (s, 3H, $H_{(10)}$).

^{13}C{^{1}H} NMR (101 MHz, $CDCl_3$): δ in ppm = 140.40 (s, $C_{(5)}$), 139.83 (s, $C_{(9)}$), 137.24 (s, $C_{(2)}$), 134.55 (s, $C_{(1)}$), 132.66 (s, $C_{(6)}$), 127.84 (s, $C_{(7)}$/$C_{(8)}$), 127.14 (s, $C_{(3)}$), 126.99 (s, $C_{(7)}$/$C_{(8)}$), 115.62 (s, $C_{(4)}$), 15.74 (s, $C_{(10)}$).

{*Re*(CO)$_4$}$_2$(BiBzIm) (**1**) [22]

To a suspension of bisbenzimidazole (94.8 mg, 0.40 mmol, 1.0 eq.) in THF (10 mL), KHMDS (0.5 M, 1.6 mL, 0.16 mg, 0.81 mmol, 2.0 eq.) was slowly added. The reaction mixture was stirred overnight at room temperature. The solvent was then removed in vacuo, and the white solid was suspended in CH_2Cl_2 (40 mL). A solution of *Re*(CO)$_5$Br (0.35 g, 0.85 mmol, 2.1 eq.) in CH_2Cl_2 (20 mL) was added dropwise. The reaction mixture was stirred for 5 days at room temperature, and the progress of the reaction was monitored by IR spectroscopy. After completion of the reaction, the mixture was filtered to remove the formed KBr. The resulting clear solution was concentrated to approximately 5 mL and the product was precipitated by addition of Et_2O (40 mL). The resulting

white solid was washed with Et_2O (20 mL) and dried in vacuo. {*Re*(CO)$_4$}2(BiBzIm) (1) was obtained as a white solid (0.30 g, 0.36 mmol, 90 %). The ^{1}H NMR spectrum agrees with the literature data [22].

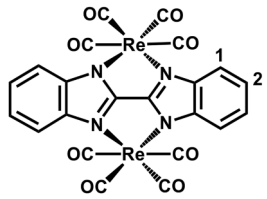

^{1}H NMR (400 MHz, CD_2Cl_2): δ in ppm = 7.69 – 7.64 (m, 4H, $H_{(2)}$), 7.41 – 7.35 (m, 4H, $H_{(1)}$).

IR (CH_2Cl_2, cm^{-1}): $\tilde{\nu}_{CO}$ = 2113 (w), 2019, 1989, 1949.

[{*Re*(CO)$_3$}$_2$(BiBzIm)-*μ*,*μ*'-(Thieno[2,3-c:5,4-c']dipyridine)]$_2$ (**2a**)

[*Re*(CO)$_4$]$_2$(BiBzIm) (1) (50.0 mg, 60.3 μmol, 2.0 eq.) and thieno[2,3-c:5,4-c']dipyridine (11.2 mg, 60.3 μmol, 2.0 eq.) were dissolved in THF (60 mL). The yellow reaction mixture was heated to reflux for 48 h. After cooling to room temperature, the orange mixture was concentrated to approx. 10 mL. A yellow solid was precipitated by the addition of Et_2O (35 mL), washed with Et_2O (2 × 5 mL) and dried in vacuo. Compound **2a** was obtained as a yellow solid (41.0 mg, 21.4 μmol, 71 %).

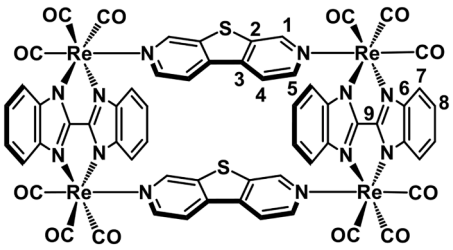

^{1}H NMR (600 MHz, CD_2Cl_2): δ in ppm = 8.59 (d, 4H, $^4J_{H,H}$ = 0.9 Hz, $H_{(1)}$), 8.09 (d, 4H, $^3J_{H,H}$ = 6.3 Hz, $H_{(4)}$), 7.89 (dd, 8H, $^3J_{H,H}$ = 6.0 Hz, $^4J_{H,H}$ = 3.1 Hz, $H_{(8)}$), 7.46 (dd, 8H, $^3J_{H,H}$ = 6.0 Hz, $^4J_{H,H}$ = 3.1 Hz, $H_{(7)}$), 7.32 (dd, 4H, $^3J_{H,H}$ = 6.3 Hz, $^4J_{H,H}$ = 0.9 Hz, $H_{(5)}$).

^{13}C{^{1}H} NMR (151 MHz, $CDCl_3$): δ in ppm = 195.25 (s, *C*O), 159.94 (s, $C_{(9)}$), 149.19 (s, $C_{(1)}$), 148.17 (s, $C_{(4)}$), 145.47 (s, $C_{(6)}$), 138.73 (s, $C_{(3)}$), 138.66 (s, $C_{(2)}$), 123.98 (s, $C_{(7)}$), 118.20 (s, $C_{(5)}$), 116.73 (s, $C_{(8)}$).

IR (CH_2Cl_2, cm^{-1}): $\tilde{\nu}_{CO}$ = 2026, 1923, 1910.

ESI MS (CH_2Cl_2): measured, 1962.9494 *m*/*z* ([*M*+HCOO]$^-$, calculated, 1962.9215 *m*/*z*).

[{*Re*(CO)$_3$}$_2$(BiBzIm)-*μ*,*μ*'-(9-(4-Methylthiophenyl)-9H-pyrrolo[2,3-c:5,4-c']dipyridine)]$_2$ (**2b**)

[*Re*(CO)$_4$]$_2$(BiBzIm) (1) (45.0 mg, 54.3 μmol, 2.0 eq.) and 9-(4-methylthiophenyl)-9H-pyrrolo[2,3-c:5,4-c']dipyridine (15.8 mg, 54.3 μmol, 2.0 eq.) were dissolved in THF (60 mL). The yellow reaction mixture was heated to reflux for 48 h. After cooling to room temperature, the solvent was removed in vacuo. The residue was washed with Et_2O (2 × 10 mL) and dried in vacuo. **2b** was obtained as a yellow solid (45.0 mg, 21.1 μmol, 78 %).

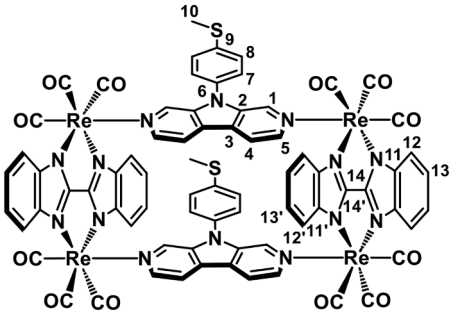

^{1}H NMR (600 MHz, CD_2Cl_2): δ in ppm = 8.32 (br s, 4H, $H_{(1)}$), 7.92 (dd, 4H, $^3J_{H,H}$ = 6.0 Hz, $^4J_{H,H}$ = 3.2 Hz, $H_{(13')}$), 7.72 (d, 4H, $^3J_{H,H}$ = 6.2 Hz, $H_{(5)}$), 7.64 (dd, 4H, $^3J_{H,H}$ = 6.0 Hz, $^4J_{H,H}$ = 3.2 Hz, $H_{(13)}$), 7.49 (dd, 4H, $^3J_{H,H}$ = 6.0 Hz, $^4J_{H,H}$ = 3.2 Hz, $H_{(12')}$), 7.33 (dd, 4H, $^3J_{H,H}$ = 6.0 Hz, $^4J_{H,H}$ = 3.2 Hz, $H_{(12)}$), 7.24 (d, 4H, $^3J_{H,H}$ = 6.2 Hz, $H_{(4)}$), 6.94 (br s, 4H, $H_{(7)}$/$H_{(8)}$), 5.89 (br s, 4H, $H_{(8)}$/$H_{(7)}$), 2.76 (s, 6H, $H_{(10)}$).

^{13}C{^{1}H} NMR (151 MHz, $CDCl_3$): δ in ppm = 196.56 (s, *C*O), 196.22 (s, *C*O), 193.62 (s, *C*O), 160.10 (s, $C_{(14')}$), 159.68 (s, $C_{(14)}$), 145.39 (s, $C_{(11')}$), 144.91 (s, $C_{(11)}$), 143.76 (s, $C_{(5)}$), 141.51 (s, $C_{(9)}$), 138.76 (s, $C_{(1)}$), 136.76 (s, $C_{(2)}$), 128.64 (s, $C_{(6)}$), 127.89 (s, $C_{(7)}$/$C_{(8)}$), 126.01 (s, $C_{(3)}$), 124.68 (s, $C_{(8)}$/$C_{(7)}$), 123.96 (s, $C_{(12')}$), 123.71 (s, $C_{(12)}$), 117.21 (s, $C_{(4)}$), 116.75 (s, $C_{(13')}$), 116.34 (s, $C_{(13)}$), 15.58 (s, $C_{(10)}$).

IR (CH_2Cl_2, cm^{-1}): $\tilde{\nu}_{CO}$ = 2024, 1920, 1906.

ESI MS (CH_2Cl_2): measured, 2173.0646 *m*/*z* ([*M*+HCOO]$^-$, calculated, 2173.0732 *m*/*z*).

Fig. 2.

CRediT authorship contribution statement

Viktoria Ebel: Writing – review & editing, Writing – original draft, Methodology, Investigation, Data curation. **Marcel Geppert:** Methodology, Investigation. **Niklas Bauch:** Investigation. **Michael Linseis:** Supervision. **Rainer F. Winter:** Writing – review & editing, Writing – original draft, Supervision, Resources, Project administration, Conceptualization.

Declaration of competing interest

The authors report no conflicts of interest for this work.

Acknowledgements

We gratefully acknowledge financial support of this work by the German Research Foundation (DFG) through Grant Number WI 1262/19–1. Thanks go to Malin Bein for ESI-MS measurements and Anke Friemel and Ulrich Haunz for their support with NMR measurements. We also thank the University of Konstanz for providing the accessories of the NMR Core Facility.

Supplementary materials

Supplementary material associated with this article can be found, in the online version, at doi:10.1016/j.jorganchem.2026.124048.

Data availability

Data will be made available on request.

References

[1] J.-M. Lehn, Supramolecular Chemistry: Concepts and Perspectives, John Wiley & Sons, 1995.
[2] E. Zangrando, M. Casanova, E. Alessio, Chem. Rev. 108 (2008) 4979–5013, https://doi.org/10.1021/cr8002449.
[3] I.V. Korendovych, R.A. Roesner, E.V. Rybak-Akimova, Adv. Inorg. Chem. 59 (2006) 109–173, https://doi.org/10.1016/S0898-8838(06)59004-X.
[4] J.-P. Zhang, X.-C. Huang, X.-M. Chen, Chem. Soc. Rev. 38 (2009) 2385–2396, https://doi.org/10.1039/b900317g.
[5] C. Müller, J.A. Whiteford, P.J. Stang, J. Am. Chem. Soc. 120 (1998) 9827–9837, https://doi.org/10.1021/ja9820801.
[6] S. Shanmugaraju, A.K. Bar, K.-W. Chi, P.S. Mukherjee, Organometallics 29 (2010) 2971–2980, https://doi.org/10.1021/om100202c.
[7] S. Shanmugaraju, S.A. Joshi, P.S. Mukherjee, Inorg. Chem. 50 (2011) 11736–11745, https://doi.org/10.1021/ic201745y.
[8] V. Martínez-Agramunt, S. Ruiz-Botella, E. Peris, Chem. Eur. J. 23 (2017) 6675–6681, https://doi.org/10.1002/chem.201700703.
[9] D.-H. Qu, Q.-C. Wang, Q.-W. Zhang, X. Ma, H. Tian, Chem. Rev. 115 (2015) 7543–7588, https://doi.org/10.1021/cr5006342.
[10] R. Custelcean, Chem. Soc. Rev. 43 (2014) 1813–1824, https://doi.org/10.1039/c3cs60371g.

[11] G. Gupta, G.S. Oggu, N. Nagesh, K.K. Bokara, B. Therrien, CrystEngComm 18 (2016) 4952–4957, https://doi.org/10.1039/c6ce00139d.
[12] Y.-R. Zheng, K. Suntharalingam, T.C. Johnstone, S.J. Lippard, Chem. Sci. 6 (2015) 1189–1193, https://doi.org/10.1039/c4sc01892c.
[13] H. Sepehrpour, W. Fu, Y. Sun, P.J. Stang, J. Am. Chem. Soc. 141 (2019) 14005–14020, https://doi.org/10.1021/jacs.9b06222.
[14] K. Acharyya, S. Bhattacharyya, H. Sepehrpour, S. Chakraborty, S. Lu, B. Shi, X. Li, P.S. Mukherjee, P.J. Stang, J. Am. Chem. Soc. 141 (2019) 14565–14569, https://doi.org/10.1021/jacs.9b08403.
[15] J.-L. Zhu, L. Xu, Y.-Y. Ren, Y. Zhang, X. Liu, G.-Q. Yin, B. Sun, X. Cao, Z. Chen, X.-L. Zhao, Nat. Commun. 10 (2019) 1–12, https://doi.org/10.1038/s41467-019-12204-7.
[16] B. Laramée-Milette, F. Nastasi, F. Puntoriero, S. Campagna, G.S. Hanan, Chem. Eur. J. 23 (2017) 16497–16504, https://doi.org/10.1002/chem.201702714.
[17] B. Laramée-Milette, N. Zaccheroni, F. Palomba, G.S. Hanan, Chem. Eur. J. 23 (2017) 6370–6379, https://doi.org/10.1002/chem.201700077.
[18] T. Rajendran, B. Manimaran, R.-T. Liao, R.-J. Lin, P. Thanasekaran, G.-H. Lee, S.-M. Peng, Y.-H. Liu, I.-J. Chang, S. Rajagopal, K.-L. Lu, Inorg. Chem. 42 (2003) 6388–6394, https://doi.org/10.1021/ic034099x.
[19] D. Donghi, G. D'Alfonso, M. Mauro, M. Panigati, P. Mercandelli, A. Sironi, P. Mussini, L. D'Alfonso, Inorg. Chem. 47 (2008) 4243–4255, https://doi.org/10.1021/ic7023692.
[20] T. Rajendran, B. Manimaran, F.-Y. Lee, G.-H. Lee, S.-M. Peng, C.M. Wang, K.-L. Lu, Inorg. Chem. 39 (2000) 2016–2017, https://doi.org/10.1021/ic9912474.
[21] D. Bhattacharya, M. Sathiyendiran, T.-T. Luo, C.-H. Chang, Y.-H. Cheng, C.-Y. Lin, G.-H. Lee, S.-M. Peng, K.-L. Lu, Inorg. Chem. 48 (2009) 3731–3742, https://doi.org/10.1021/ic8024099.
[22] K.D. Benkstein, C.L. Stern, J.T. Hupp, Angew. Chem. Int. Ed. 39 (2000) 2891–2893, https://doi.org/10.1002/1521-3773(20000818)39:16<2891::AID−NIE2891>3.0.CO;2-Q.
[23] P. Thanasekaran, C.-C. Lee, K.-L. Lu, Acc. Chem. Res. 45 (2012) 1403–1418, https://doi.org/10.1021/ar200243w.
[24] G. Li, L. Xu, W. Zhang, K. Zhou, Y. Ding, F. Liu, X. He, G. He, Angew. Chem. Int. Ed. 57 (2018) 4897–4901, https://doi.org/10.1002/anie.201711761.
[25] R. Nagarajaprakash, D. Divya, B. Ramakrishna, B. Manimaran, Organometallics 33 (2014) 1367–1373, https://doi.org/10.1021/om400776m.
[26] G.-X. Jin, T. Wang, Y. Sun, Y.-L. Li, J.-P. Ma, Inorg. Chem. 59 (2020) 15019–15027, https://doi.org/10.1021/acs.inorgchem.0c01845.
[27] S.-S. Sun, A.J. Lees, J. Am. Chem. Soc. 122 (2000) 8956–8967, https://doi.org/10.1021/ja001677p.
[28] B. Manimaran, P. Thanasekaran, T. Rajendran, R.-J. Lin, I.-J. Chang, G.-H. Lee, S.-M. Peng, S. Rajagopal, K.-L. Lu, Inorg. Chem. 41 (2002) 5323–5325, https://doi.org/10.1021/ic020364.
[29] A. Ramdass, V. Sathish, B. Manimaran, P. Thanasekaran, S. Rajagopal, Orient. J. Chem. 32 (2016) 1859–1873, https://doi.org/10.13005/ojc/320413.
[30] P.H. Dinolfo, J.T. Hupp, J. Am. Chem. Soc. 126 (2004) 16814–16819, https://doi.org/10.1021/ja045457d.
[31] P.H. Dinolfo, M.E. Williams, C.L. Stern, J.T. Hupp, J. Am. Chem. Soc. 126 (2004) 12989–13001, https://doi.org/10.1021/ja0473182.
[32] P.H. Dinolfo, S.J. Lee, V. Coropceanu, J.-L. Brédas, J.T. Hupp, Inorg. Chem. 44 (2005) 5789–5797, https://doi.org/10.1021/ic050834o.
[33] K.N. Solov'ev, E.A. Borisevich, Phys.-Uspekhi 48 (2005) 231, https://doi.org/10.1070/PU2005v048n03ABEH001761.
[34] S.M. Parke, E. Rivard, Isr. J. Chem. 58 (2018) 915–926, https://doi.org/10.1002/ijch.201800039.
[35] P.-T. Chou, Y. Chi, M.-W. Chung, C.-C. Lin, Coord. Chem. Rev. 255 (2011) 2653–2665, https://doi.org/10.1016/j.ccr.2010.12.013.
[36] J. Ohshita, K. Murakami, D. Tanaka, Y. Ooyama, T. Mizumo, N. Kobayashi, H. Higashimura, T. Nakanishi, Y. Hasegawa, Organometallics 33 (2014) 517–521, https://doi.org/10.1021/om401019b.
[37] P.S. Braterman, Metal Carbonyl Spectra, Academic Press, Glasgow, Scotland, 1975.
[38] P.S. Braterman, J.I. Song, J. Org. Chem. 56 (1991) 4678–4682, https://doi.org/10.1021/jo00015a021.
[39] J.E. O'Reilly, P.J. Elving, J. Am. Chem. Soc. 94 (1972) 7941–7949, https://doi.org/10.1021/ja00778a001.
[40] D. Gosztola, M.P. Niemczyk, W. Svec, A.S. Lukas, M.R. Wasielewski, J. Phys. Chem. A 104 (2000) 6545–6551, https://doi.org/10.1021/jp000706f.
[41] R.F. Winter, Organometallics 33 (2014) 4517–4536, https://doi.org/10.1021/om500029x.
[42] M.B. Robin, P. Day, Adv. Inorg. Chem. Radiochem. 10 (1968) 247–422, https://doi.org/10.1016/S0065-2792(08)60179-X.
[43] K.D. Benkstein, C.L. Stern, K.E. Splan, R.C. Johnson, K.A. Walters, F. W. Vanhelmont, J.T. Hupp, Eur. J. Inorg. Chem. 2002 (2002) 2818–2822, https://doi.org/10.1002/1099-0682(200211)2002:11<2818::AID−JIC2818>3.0.CO;2-1.
[44] G.U. Bublitz, W.M. Laidlaw, R.G. Denning, S.G. Boxer, J. Am. Chem. Soc. 120 (1998) 6068–6075, https://doi.org/10.1021/ja980453s.
[45] L.N. Silverman, P. Kanchanawong, T.P. Treynor, S.G. Boxer, Phil. Trans. R. Soc. A. 366 (2008) 33–45, https://doi.org/10.1098/rsta.2007.2137.
[46] C.G. Atwood, W.E. Geiger, J. Am. Chem. Soc. 122 (2000) 5477–5485, https://doi.org/10.1021/ja994064p.
[47] M.E. Stoll, S.R. Lovelace, W.E. Geiger, H. Schimanke, I. Hyla-Kryspin, R. Gleiter, J. Am. Chem. Soc. 121 (1999) 9343–9351, https://doi.org/10.1021/ja9914792.
[48] M. Krejčik, M. Daněk, F. Hartl, J. Electroanal. Chem. 317 (1991) 179–187, https://doi.org/10.1016/0022-0728(91)85012-E.
[49] P.H. Dinolfo, K.D. Benkstein, C.L. Stern, J.T. Hupp, Inorg. Chem. 44 (2005) 8707–8714, https://doi.org/10.1021/ic050894u.
[50] N.S. Hush, in: F.A. Cotton (Ed.), Progress in Inorganic Chemistry, Progress in Inorganic Chemistry, 72, Interscience, New York, 1967, pp. 391–444.
[51] N.S. Hush, M.N. Paddon-Row, E. Cotsaris, H. Oevering, J.W. Verhoeven, M. Heppener, Chem. Phys. Lett. 117 (1985) 8–11, https://doi.org/10.1016/0009-2614(85)80394-8.
[52] T. Rajendran, B. Manimaran, F.-Y. Lee, P.-J. Chen, S.-C. Lin, G.-H. Lee, S.-M. Peng, Y.-J. Chen, K.-L. Lu, J. Chem. Soc., Dalton Trans (2001) 3346–3351, https://doi.org/10.1039/b101992i.
[53] S.A. Lermontova, M.V. Arsenyev, A.V. Cherkasov, G.K. Fukin, A.V. Afanasyev, A. V. Yudintsev, I.S. Grigoryev, E.Y. Ladilina, T.S. Lyubova, N.Y. Shilyagina, I. V. Balalaeva, L.G. Klapshina, A.V. Piskunov, Int. J. Mol. Sci. 24 (2023) 5818, https://doi.org/10.3390/ijms24065818.
[54] B. Xu, N.J. Tao, Science 301 (2003) 1221–1223, https://doi.org/10.1126/science.1087481.
[55] L. Venkataraman, J.E. Klare, C. Nuckolls, M.S. Hybertsen, M.L. Steigerwald, Nature 442 (2006) 904–907, https://doi.org/10.1038/nature05037.
[56] L. Venkataraman, J.E. Klare, I.W. Tam, C. Nuckolls, M.S. Hybertsen, M. L. Steigerwald, Nano Lett 6 (2006) 458–462, https://doi.org/10.1021/nl052373.
[57] A. Mang, N. Rotthowe, K. Beltako, M. Linseis, F. Pauly, R.F. Winter, Nanoscale 15 (2023) 5305–5316, https://doi.org/10.1039/d2nr05670d.
[58] M. Nau, W. Bro-Jørgensen, M. Linseis, M. Bodensteiner, R.F. Winter, G.C. Solomon, Angew. Chem. Int. Ed. 137 (2025) e202417796, https://doi.org/10.1002/anie.202417796.
[59] C.J.M. Magoga, Phys. Rev. B (1999) 16011, https://doi.org/10.1103/PhysRevB.59.16011.
[60] H. Vazquez, R. Skouta, S. Schneebeli, M. Kamenetska, R. Breslow, L. Venkataraman, M.S. Hybertsen, Nat. Nanotechnol. 7 (2012) 663–667, https://doi.org/10.1038/nnano.2012.147.
[61] M.J. Frisch, G.W. Trucks, H.B. Schlegel, G.E. Scuseria, M.A. Robb, J.R. Cheeseman, G. Scalmani, V. Barone, G.A. Petersson, H. Nakatsuji, X. Li, M. Caricato, A.V. Marenich, J. Bloino, B.G. Janesko, R. Gomperts, B. Mennucci, H.P. Hratchian, J.V. Ortiz, A.F. Izmaylov, J.L. Sonnenberg, D. Williams-Young, F. Ding, F. Lipparini, F. Egidi, J. Goings, B. Peng, A. Petrone, T. Henderson, D. Ranasinghe, V.G. Zakrzewski, J. Gao, N. Rega, G. Zheng, W. Liang, M. Hada, M. Ehara, K. Toyota, R. Fukuda, J. Hasegawa, M. Ishida, T. Nakajima, Y. Honda, O. Kitao, H. Nakai, T. Vreven, K. Throssell, J.A. Montgomery Jr., J.E. Peralta, F. Ogliaro, M.J. Bearpark, J.J. Heyd, E.N. Brothers, K.N. Kudin, V.N. Staroverov, T.A. Keith, R. Kobayashi, J. Normand, K. Raghavachari, A.P. Rendell, J.C. Burant, S.S. Iyengar, J. Tomasi, M. Cossi, J.M. Millam, M. Klene, C. Adamo, R. Cammi, J.W. Ochterski, R.L. Martin, K. Morokuma, O. Farkas, J.B.F. and, D.J. Fox, Gaussian 16, Revision B.01. 2016, Wallingford CT.
[62] M. Cossi, N. Rega, G. Scalmani, V. Barone, J. Comput. Chem. 24 (2003) 669–681, https://doi.org/10.1002/jcc.10189.
[63] J.P. Perdew, K. Burke, M. Ernzerhof, Phys. Rev. Lett. 77 (1996) 3865–3868, https://doi.org/10.1103/PhysRevLett.77.3865.
[64] N.M. O'Boyle, A.L. Tenderholt, K.M. Langner, J. Comput. Chem. 29 (2008) 839–845, https://doi.org/10.1002/jcc.20823.
[65] M.D. Hanwell, D.E. Curtis, D.C. Lonie, T. Vandermeersch, E. Zurek, G.R. Hutchison, J. Cheminform. 4 (2012) 17, https://doi.org/10.1186/1758-2946-4-17.
[66] W. Humphrey, A. Dalke, K. Schulten, J. Mol. Graph. 14 (1996) 33–38, https://doi.org/10.1016/0263-7855(96)00018-5.
[67] Povray.org (accessed 08.08. https://www.povray.org/download/, 2025 (accessed 08.08.)
[68] S. Durben, T. Baumgartner, Angew. Chem. Int. Ed. 50 (2011) 7948–7952, https://doi.org/10.1002/anie.201102453.